Improved High Efficiency Organic Solar Cells via Incorporation of a Conjugated Polyelectrolyte Interlayer

Supporting Information

Jung Hwa Seo,[†] Andrea Gutacker,[‡] Yanming Sun, Hongbin Wu,[§] Fei Huang,[§] Yong Cao,[§] Ullrich Scherf,[‡] Alan J. Heeger,[†] Guillermo C. Bazan[*,†]*

Center for Polymers and Organic Solids, Department of Physics and Chemistry & Biochemistry, University of California, Santa Barbara, California 93106 and Bergische Universitaet Wuppertal, Makromolekulare Chemie, Wuppertal, Germany, Institute of Polymer Optoelectronic Materials and Devices, South China University of Technology, Guangzhou 510640, P. R. China

1. Experimental Methods

Solar Cell Fabrication: Solar cells were fabricated by spin-casting the blended films onto a 40 nm layer of PEDOT:PSS onto patterned ITO glass substrates. Blended films of PCDTBT:$PC_{71}BM$ (1:4 ratio) were spin cast at 5000 rpm for 40 sec from a mixture solution in chlorobenzene and 1,2-dichlorobenzene (1:3 ratio) onto the PEDOT:PSS layer. The films were annealed on a hot plate at 70˚C for 10 min in a glove box. The CPE layers were subsequently deposited by spin casting from 0.01% (w/v) **P3TMAHT** and 0.02% (w/v) **PF2/6-*b*-P3TMAHT** methanol solutions. Finally, 100 nm thick Al electrodes were deposited by thermal evaporation in a vacuum. *J–V* characteristics of all devices were measured using a Keithley 236 Source Measure Unit. Solar cell performance used an Air Mass 1.5 Global (AM 1.5 G) solar simulator with an irradiation intensity of 100 mW/cm^2. An aperture (9.84

mm^2) was used on top of the cell to eliminate extrinsic effects such as crosstalk, wave guiding, shadow effects. The spectral mismatch factor was calculated by comparison of the solar simulator spectrum and the AM 1.5 spectrum at RT.

Surface topography: Atomic force microscopy was carried out for surface topography. A platinum-iridium coated Si probe (Veeco, SCM-PIT) with a resonant frequency around 72 kHz was used. All data were measured under the N_2 atmosphere and by using the same tip using a Multimode microscope with a Nanoscope controller IIIa (Veeco).

Materials: The polythiophene homopolymer **P3TMAHT** and the ionic diblock copolymer **PF2/6-*b*-P3TMAHT** have been prepared from the corresponding non-ionic 6-bromohexyl substituted precursors (**P3HBrHT** and **PF2/6-*b*-P3HBrT**) following precedures described in the literature.[1] The molecular weights (GPC, sovents: toluene, THF; PS calibration) of the non ionic homopolymer (**P3HBrHT**) and block copolymer (**PF2/6-*b*-P3HBrT**) precursors are given below.

P3HBrHT: Mn: 8000, Mw: 14000, PDI: 1.75, l~33.

PF2/6-*b*-P3HBrT: Mn: 13000, Mw: 18000, PDI: 1.38, (**P3BrHT block**: Mn: 6500, Mw: 9100, PDI: 1.40), resulting in n ~16, m ~27.

2. UPS and UV-Vis Absorption Spectroscopy

Figure S1 shows the UPS spectra taken for **P3TMAHT** and **PF2/6-*b*-P3TMAHT** films. In the left-hand side of Fig. S1(a), the high binding energy cutoff from a spectrum is E_{cutoff}, which is determined by linear extrapolation to zero at the yield of secondary electrons.[2,3] The right side of Fig. S1(a) shows the HOMO region. The E_{HOMO} is the onset relative to the Fermi level (E_F) of Au (at 0 eV), where the E_F was determined from the Au substrate. From Fig. S1(a), the ionization potential (*IP*, HOMO) is determined by using the incident photon energy ($h\nu$ =21.2 eV) for He I, E_{cutoff}, and E_{HOMO} according to the equation, $IP = h\nu - (E_{cutoff} - E_{HOMO})$.[4,5]

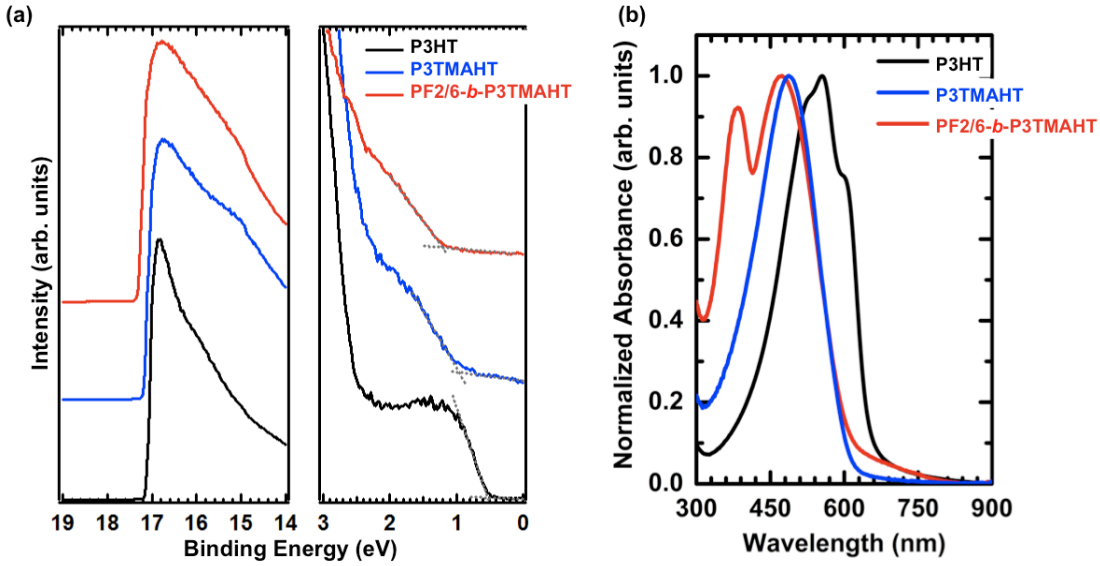

Figure S1. (a) UPS Spectra and (b) UV-Vis absorption spectra of **P3TMAHT** and **PF2/6-b-P3TMAHT** films. Spectra of P3HT for a comparison.

The electron affinity (*EA*, LUMO) is estimated by using the HOMO and the optical gap from the UV-Vis absorption spectra from Fig. S1(b). The absorption spectra were taken from each CPE film on a glassquartz substrate. The uncertainty of the *EA* is due to a difference between the true gap and the optical gap by the exciton binding energy.[2-6] With such uncertainty, the values obtained from UPS and UV-Vis absorption spectra are summarized in Table S1.

Table S1. Energy levels of P3HT, **P3TMAHT**, and **PF2/6-*b*-P3TMAHT**.

	Eg (UV-Vis)	HOMO (UPS)	LUMO (Eg)
P3HT	**1.90**	**4.6**	**2.70**
P3TMAHT	**2.05**	**4.98**	**2.93**
PF2/6-*b*-P3TMAHT	**2.02**	**5.06**	**3.04**

3. Dark current characteristics.

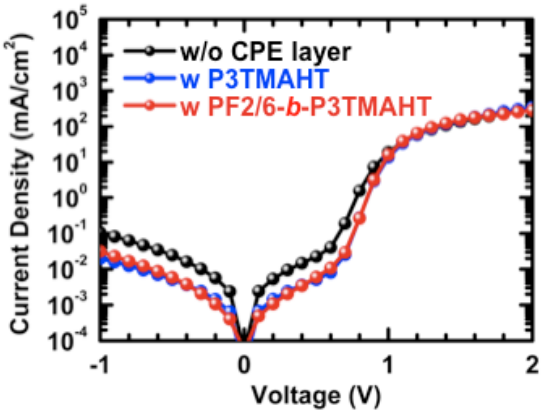

Figure S2. Semiloarithmic *J-V* characteristics of the devices under dark conditions.

4. Surface potential images of CPE on PCDTBT:$PC_{71}BM$ bilayers.

Figure S2 shows the surface morphologies obtained by AFM and surface potential profiles obtained by using scanning Kelvin probe force microscopy (SKPM), respectively. A platinum-iridium coated Si probe (Veeco, SCM-PIT) with a resonant frequency around 72 kHz was used in this experiment. Topography and surface potential scans were recorded at the same time in the interleave scan mode at a fixed lift height of 50 nm above the surface. As the scanning tip approaches the surface, an electric field is generated due to the differential potential between the tip and the surface. The backing voltage applied to the tip to nullify the field provides a relative measure of the surface potential.[7] All data were measured under the N_2 atmosphere and by using the same tip.

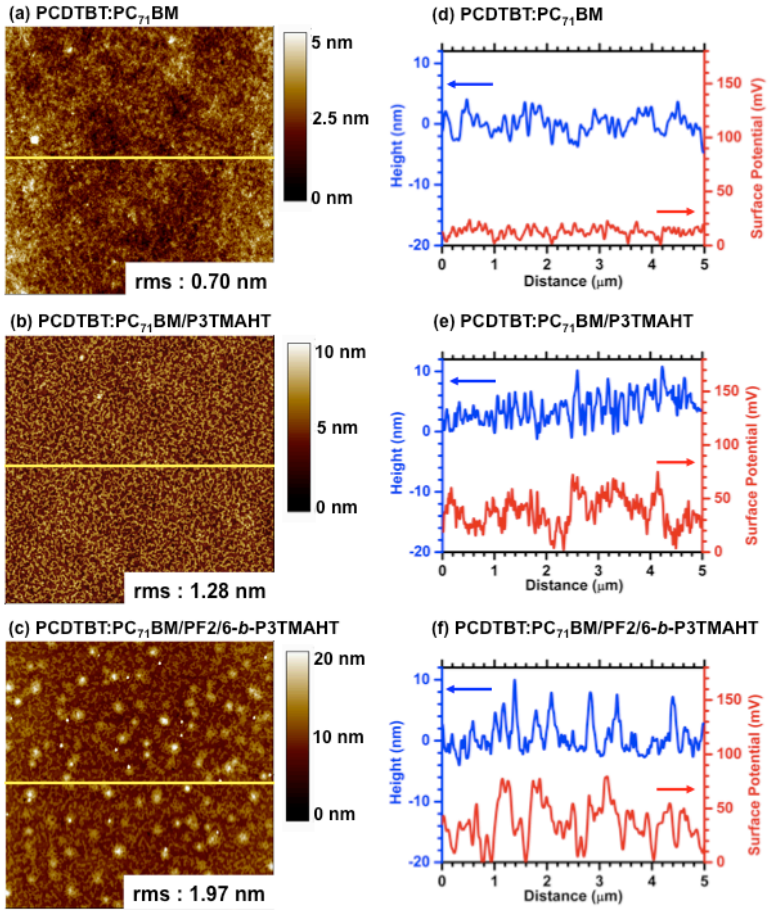

Figure S3. Surface topographic AFM images (size : 5 μm × 5 μm) of (a) the control device with no CPE layer, (b) **P3TMAHT** on PCDTBT:$PC_{71}BM$ layer, where the CPE was deposited from 0.01% solution, and (c) **PF2/6-*b*-P3TMAHT** on PCDTBT/$PC_{71}BM$ layer, where the CPE was deposited from 0.02% solution. (d)-(f) Surface potential profiles corresponding to (a)-(c).

Fig. S2(d)-(f) shows the height distribution and surface potential along the directions highlighted in yellow in Fig. S2(a)-(c). The PCDTBT:$PC_{71}BM$ surface exhibits variations potential of ~ 15 mV. Fig. S2(e) and S2(f) show that the CPE layers increase the surface potential by as much as 60 mV with sharp peaks along the scan direction. The increased surface potential is attributed to the local electrostatic field provided by the ionic component in the CPE layer.

References

(1) (a) Gutacker, A.; Adamczyk, S.; Helfer, A.; Garner, L. E.; Evans, R. C; Fonseca, S. M.; Knaapila, M.; Bazan, G. C.; Burrows, H. D.; Scherf, U. *J. Mater. Chem.* **2010**, *20*, 1423. (b) Knaapila, M.; Evans, R. C.; Garamus, V. M.; Almásy, L.; Székely, N. K.; Gutacker, A.; Scherf, U.; Burrows, H. D. *Langmuir* **2010**, *26*, 15634. (c) Tu, G.; Li, H.; Forster, M.; Heiderhoff, R.; Balk, L. J.; Sigel, R.;. Scherf, U. *Small* **2007**, *3*, 1001.

(2) Braun, S.; Salaneck, W. R.; Fahlman, M. Adv. *Mater.* **2009**, *21*, 1450.

(3) Seo, J. H.; Yang, R.; Brzezinski, J. Z.; Walker, B.; Bazan, G, C.; Nguyen, T.-Q. *Adv. Mater.* **2009**, *21*, 1006.

(4) Gao, Y. *Acc. Chem. Res.* **1999**, *32*, 247.

(5) Ishii, H.; Sugiyama, K.; Ito, E.; Seki, K. *Ad*v. *Mater.* **1999**, *11*, 605.

(6) Hwang, J.; Wan, A.; Kahn. A. *Mater. Sci. Engineer. R* **2009**, *64*, 1.

(7) Li, H.; Xu, Y.; Hoven, C. V.; Li, C.; Seo, J. H.; Bazan, G. C. *J. Am. Chem. Soc.* **2009**, *131*, 8903.